IJMMM International Journal of Minerals, Metallurgy and Materials 矿物冶金与材料学报（英文版）

# Influence of substituting $B_2O_3$ with $Li_2O$ on the viscosity, structure and crystalline phase of low-reactivity mold flux

Rongzhen Mo, Xubin Zhang, Ying Ren, Junjie Hu, and Lifeng Zhang

Cite this article as:
Rongzhen Mo, Xubin Zhang, Ying Ren, Junjie Hu, and Lifeng Zhang, Influence of substituting $B_2O_3$ with $Li_2O$ on the viscosity, structure and crystalline phase of low-reactivity mold flux, *Int. J. Miner. Metall. Mater.*, 30(2023), No. 7, pp. 1320-1328. https://doi.org/10.1007/s12613-023-2621-x

View the article online at SpringerLink or IJMMM Webpage.

---

*International Journal of Minerals, Metallurgy and Materials*
*Volume 30, Number 7, July 2023, Page 1320*
**https://doi.org/10.1007/s12613-023-2621-x**

# Influence of substituting $B_2O_3$ with $Li_2O$ on the viscosity, structure and crystalline phase of low-reactivity mold flux

*Rongzhen Mo*[1)], *Xubin Zhang*[2)], *Ying Ren*[1),✉], *Junjie Hu*[1)], *and Lifeng Zhang*[3),✉]

1) School of Metallurgical and Ecological Engineering, University of Science and Technology Beijing, Beijing 100083, China
2) Lecture at College of Materials Science and Engineering, Chongqing University, Chongqing 400030, China
3) School of Mechanical and Materials Engineering, North China University of Technology, Beijing 100144, China
(Received: 7 October 2022; revised: 28 February 2023; accepted: 1 March 2023)

**Abstract:** The low-reactivity mold flux with low $SiO_2$ content is considered suitable for the continuous casting of high-aluminum steel since it can significantly reduce the reaction between Al in steel and $SiO_2$ in mold flux. However, the traditional low-reactivity mold flux still presents some problems such as high viscosity and strong crystallization tendency. In this study, the co-addition of $Li_2O$ and $B_2O_3$ in CaO–$Al_2O_3$–10wt%$SiO_2$ based low-reactivity mold flux was proposed to improve properties of mold flux for high-aluminum steel, and the effect of $Li_2O$ replacing $B_2O_3$ on properties of mold flux was investigated. The viscosity of the mold flux with 2wt% $Li_2O$ and 6wt% $B_2O_3$ reached a minimum value of 0.07 Pa·s. The break temperature and melting point showed a similar trend with the viscosity. Besides, the melt structure and precipitation of the crystalline phase were studied using Raman and X-ray diffraction spectra to better understand the evolution of viscosity. It demonstrated that with increasing $Li_2O$ content in the mold flux from 0 to 6wt%, the degree of polymerization of aluminate and the aluminosilicate network structure increased because of increasing $Li^+$ released by $Li_2O$, indicating the added $Li_2O$ was preferentially associated with $Al^{3+}$ as a charge compensator. The precipitation of $LiAlO_2$ crystalline phase gradually increased with the replacement of $B_2O_3$ by $Li_2O$. Therefore, $Li_2O$ content should be controlled below 2wt% to avoid $LiAlO_2$ precipitation, which was harmful to the continuous casting of high-aluminum steels.

**Keywords:** low-reactivity mold flux; viscosity; structure; crystalline phase

## 1. Introduction

High-aluminum steel contains 0.5wt%–2.5wt% dissolved aluminum [1], which is widely used in automotive, shipping, and other fields because of its lightweight, high strength, and good plasticity. However, the continuous casting process of high-aluminum steel is restricted by the steel–slag interface reaction [2–3]. The reactive CaO–$SiO_2$-based mold flux brings difficulty in avoiding the strong reaction at the steel–slag interface between Al and $SiO_2$ [4–8]. As a result, the viscosity of mold flux increases, the surface quality of the slab reduces, and the smooth continuous casting process harms [9–10]. Street *et al.* [11] proposed a nonreactive CaO–$Al_2O_3$-based mold flux without $SiO_2$ to prevent the interface reaction. However, it greatly lowered glass properties and increased the crystallization tendency of the mold flux. Therefore, for a long time, reactive and nonreactive mold fluxes were barely used to cast high-aluminum steel continuously. Afterwards, the low-reactivity mold flux with a certain amount of $SiO_2$ was proposed, which helped weaken the steel–slag interface reaction and maintained glass properties of the mold flux.

Fig. 1 summarizes the reduction of $SiO_2$ content and the required time for reaction equilibrium during the continuous casting of high-aluminum steel for different compositions of mold flux. When the initial $SiO_2$ content of the mold flux was approximately 35wt%, 18wt%, and 10wt%, more than 57%, approximately 55%, and less than 40% $SiO_2$ was decreased, respectively, after the equilibrium reaction between steel and mold flux. It means that the CaO–$Al_2O_3$–10wt%$SiO_2$ low-reactivity mold flux can substantially alleviate the steel–slag interface reaction.

However, the low-reactivity mold flux also presented some problems, such as high viscosity and strong crystallization tendency. Thus, most researchers tried to improve its properties by optimizing the composition of the mold flux, such as addition $B_2O_3$ or $Li_2O$. Table 1 presents the variation trend of properties for some low-reactivity mold flux with increasing $B_2O_3$ or $Li_2O$ content [7,15–16,18–31]. It was well-known that the addition of $B_2O_3$ effectively improve properties of mold flux [18–23], but the excessive addition of $B_2O_3$ to the mold flux significantly promoted the interface reaction between Al and $B_2O_3$, leading to the fluctuation in mold flux properties [15–16]. Besides, a moderate amount of $Li_2O$ in the mold flux was more obviously beneficial to lower the melting point, reduce the viscosity, and weaken the crystal-

✉ Corresponding authors: Ying Ren E-mail: yingren@ustb.edu.cn; Lifeng Zhang E-mail: zhanglifeng@ncut.edu.cn

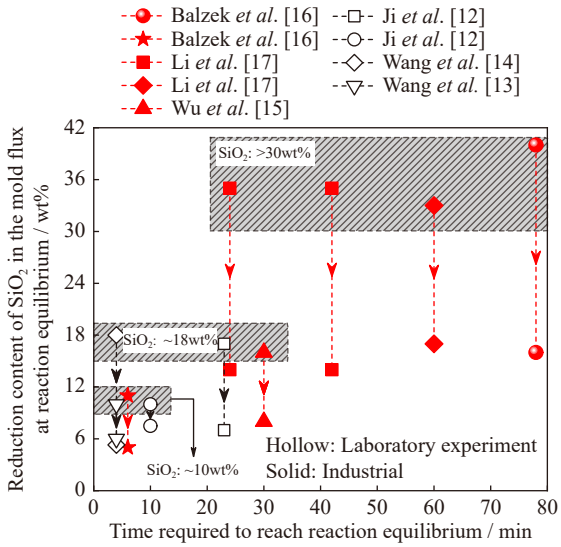


**Fig. 1. Reduction content of $SiO_2$ and the required time for reaction equilibrium during the continuous casting of high-aluminum steel using the low-reactivity mold flux [12–17].**

lization tendency [24–26], but excessive addition in the $Li_2O$ content of the mold flux promoted the precipitation of high melting point crystalline phase $LiAlO_2$, which would deteriorate properties of mold flux [27–29]. It was noted that the $Li_2O$ in the mold flux does not participate in the steel–slag reaction [7,15,30], so maybe replacing $B_2O_3$ with moderate $Li_2O$ in the mold flux not only improved properties of the mold flux, but also alleviated the interface reaction between Al and $B_2O_3$. A few studies on substituting $Li_2O$ for $B_2O_3$ in the mold flux have been reported [13,15] and a suitable content of $Li_2O$ in the low-reactivity mold flux for $LiAlO_2$ formation need further research especially with different $B_2O_3$ contents.

In this study, the effect of submitting $B_2O_3$ with different $Li_2O$ content on the viscosity, structure, and crystalline phase of a CaO–$Al_2O_3$–10wt%$SiO_2$ low-reactivity mold flux was researched systemically to obtained the best ratio of $B_2O_3$ and $Li_2O$. Besides, the crystallization behavior of $Li_2O$ in the $B_2O_3$-contianing CaO–$Al_2O_3$–10wt%$SiO_2$ mold flux was investigated.

## 2. Experimental

The mold flux was prepared using the reagent-grade powders of CaO, $SiO_2$, $Al_2O_3$, $BaCO_3$, $CaF_2$, $Li_2CO_3$, and $B_2O_3$. CaO powder was calcined at 1000°C for 5 h in a muffle furnace to decompose carbonate and hydroxide. The powders of $SiO_2$, $Al_2O_3$, $BaCO_3$, $CaF_2$, $Li_2CO_3$, and $B_2O_3$ were heated at 500°C for 2 h. Mixed powders were melted at 1400°C for 0.5 h in a graphite crucible to homogenize the chemical composition and eliminate bubbles. Ar gas with a purity of 99.999% was blown at a flow rate of 0.5 L/min. Samples were quenched in water and grounded into powders with a diameter smaller than 75 μm. The mold flux compositions were analyzed using X-ray fluoroscopy and inductively coupled plasma atomic emission spectrometry. The composition of the mold flux before and after pre-melting was almost identical, as listed in Table 2.

Rotational viscometry was used to investigate mold flux viscosity. The details of the experimental apparatus were presented in a previous study [19]. After the calibration measurement of the viscometer, a 250-g pre-melted sample was added to a graphite crucible at 1200°C in a $MoSi_2$ heating furnace. Samples were heated at 1300°C for 20 min to obtain a homogeneous melt under an Ar atmosphere at a flow rate of 0.5 L/min. The cylinder was slowly submerged into

**Table 1. Effect of $B_2O_3$ and $Li_2O$ on CaO–$Al_2O_3$-based mold flux properties [7,15–16,18–31]**

| Authors | Additive | Additive amount / wt% | Slag | Melting point | Viscosity | Crystallization | Reaction | Year |
|---|---|---|---|---|---|---|---|---|
| Wang *et al.* [18] | $B_2O_3$ | 0–4 | CaO–8wt%$SiO_2$–$Al_2O_3$ | ↓ | ↓ | | | 2011 |
| Li *et al.* [19] | $B_2O_3$ | 8–12 | CaO–$Al_2O_3$ | ↓ | ↓ | ↓ | | 2017 |
| Yan *et al.* [20] | $B_2O_3$ | 10–20 | CaO–5wt%$SiO_2$–$Al_2O_3$ | | ↓ | | | 2017 |
| Yan *et al.* [21] | $B_2O_3$ | 10–20 | CaO–5wt%$SiO_2$–$Al_2O_3$ | | | ↓ | | 2016 |
| Yu *et al.* [22] | $B_2O_3$ | 4–10 | CaO–6wt%$SiO_2$–$Al_2O_3$ | ↓ | ↓ | ↓ | | 2011 |
| Huang *et al.* [23] | $B_2O_3$ | 0–9 | CaO–6wt%$SiO_2$–$Al_2O_3$ | | ↓ | | | 2013 |
| Blazek *et al.* [16] | $B_2O_3$ | 10–16 | CaO–$SiO_2$–$Al_2O_3$ | | | | React | 2011 |
| Wu *et al.* [15] | $B_2O_3$ | 18 | CaO–$SiO_2$–$Al_2O_3$ | | | | React | 2016 |
| Kim *et al.* [24] | $Li_2O$ | 0–4 | CaO–$Al_2O_3$ | | ↓ | | | 2012 |
| Wu *et al.* [25] | $Li_2O$ | 5–8 | CaO–$Al_2O_3$ | ↓↑ | ↓↑ | | | 2012 |
| Li *et al.* [26] | $Li_2O$ | 0–8 | CaO–$Al_2O_3$ | | | ↓ | | 2018 |
| Qi *et al.* [27] | $Li_2O$ | 10–18 | CaO–$Al_2O_3$ | | ↓ | | | 2017 |
| Zhou *et al.* [28] | $Li_2O$ | 0–6 | CaO–9wt%$SiO_2$–$Al_2O_3$ | ↓ | | ↓↑ | | 2018 |
| Lu *et al.* [29] | $Li_2O$ | 2–7 | CaO–11wt%$SiO_2$–$Al_2O_3$ | | | ↓* | | 2014 |
| Qi *et al.* [30] | $Li_2O$ | 10–18 | CaO–2wt%$SiO_2$–$Al_2O_3$ | | ↓↑ | ↑ | | 2016 |
| Wu *et al.* [15] | $Li_2O$ | ~2 | CaO–5wt%$SiO_2$–$Al_2O_3$ | | | | Non-react | 2016 |
| Yang *et al.* [7,31] | $Li_2O$ | ~2 | CaO–7wt%$SiO_2$–$Al_2O_3$ | | | | Non-react | 2019 |

Note: ↓— decrease; ↑—increase; ↓↑—initial decrease and then increase; *—in the high temperature zone; blank indicates there are no relevant results shown in the reference; reaction means the reaction between steel and $B_2O_3$ or $Li_2O$ in mold flux.

**Table 2. Compositions of different mold flux** wt%

| Sample | Before pre-melting | | | | | | | After pre-melting | | | | | | |
|---|---|---|---|---|---|---|---|---|---|---|---|---|---|---|
| | CaO | $SiO_2$ | $Al_2O_3$ | BaO | $CaF_2$ | $Li_2O$ | $B_2O_3$ | CaO | $SiO_2$ | $Al_2O_3$ | BaO | $CaF_2$ | $Li_2O$ | $B_2O_3$ |
| S-LB-1 | 26.00 | 10.00 | 26.00 | 10.00 | 20.00 | 0 | 8.00 | 27.72 | 9.52 | 26.57 | 9.92 | 18.85 | 0 | 7.42 |
| S-LB-2 | 26.00 | 10.00 | 26.00 | 10.00 | 20.00 | 2.00 | 6.00 | 27.50 | 9.69 | 26.45 | 9.79 | 19.08 | 1.92 | 5.55 |
| S-LB-3 | 26.00 | 10.00 | 26.00 | 10.00 | 20.00 | 4.00 | 4.00 | 27.27 | 9.59 | 26.66 | 9.70 | 19.19 | 4.00 | 3.60 |
| S-LB-4 | 26.00 | 10.00 | 26.00 | 10.00 | 20.00 | 6.00 | 2.00 | 27.27 | 9.75 | 26.58 | 10.01 | 18.80 | 5.95 | 1.64 |

the mold flux at a rotational rate of 12 r/min for the viscosity measurement. The melt was cooled at a rate of 6°C/min until the recorded viscosity approached 3 Pa·s.

The melting point was determined using the hemisphere melting point method. Alcohol was used to cement a 2-g sample of pre-melting powder into a cylinder with an inner radius of 3 mm and a height of 3 mm. The cylinder was placed in a furnace at 800°C and heated on a corundum plate at a rate of 25°C/min. The hemispherical temperature was recorded automatically when the cylinder height decreased to half of the original height. Precipitated crystalline phases in mold fluxes quenched at 950°C and 1150°C were identified using X-ray diffraction (XRD) (Rigaku-TTR III, Rigaku Corporation, Japan). The XRD data were collected in a range of 10°–80° at a rate of 2°/s.

To identify the high-temperature melt structure at 1300°C, flux samples were quenched on a water-cooled copper plate for Raman spectrum (LabRAM HR800, Horiba Jobin Yvon, France) measurements. The quenched sample was taken from the crucible before the viscosity test. XRD results confirmed the glassy structure of quenched fluxes, as shown in Fig. 2. The Raman spectra were observed between 400 and 1600 $cm^{-1}$ through a 514-nm excitation source laser. The spectrum data were background subtracted and deconvoluted with the Gaussian function.

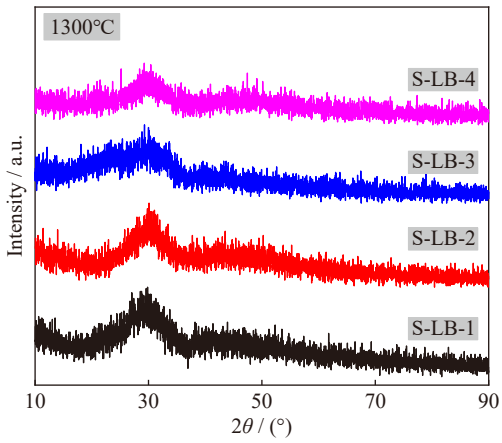


**Fig. 2. XRD results of the as-quenched slag at 1300°C.**

## 3. Results and discussion

### 3.1. Effect of substituting $Li_2O$ for $B_2O_3$ on the viscosity and melting point of the mold flux

The viscosity of the mold flux with the substitution of $Li_2O$ for $B_2O_3$ at different temperatures is shown in Fig. 3. Fig. 4 presents the viscosity–temperature curves of the mold flux, which reflect the crystallization trend of the mold flux during cooling. With increasing $Li_2O$ content in the mold flux, the viscosity first decreased and then obviously increased, particularly in the low-temperature zone. When it contained 2wt% $Li_2O$ and 6wt% $B_2O_3$, the mold flux had a minimum viscosity of 0.07 Pa·s at 1300°C. When the mold flux contained 8wt% $B_2O_3$ (without $Li_2O$) or 6wt% $Li_2O$ (i.e., 2wt% $B_2O_3$), the mold flux viscosity was 0.19 Pa·s or 0.34 Pa·s, respectively. Wang [13] found that 1.8wt% $Li_2O$ and 7.2wt% $B_2O_3$ contained in the mold flux reduced the viscosity of the mold flux, consistent with the current results. Therefore, a combined addition of $Li_2O$ and $B_2O_3$ to mold flux was beneficial to effectively reduce the mold flux viscosity.

Seetharaman *et al.* [32] proposed a mathematical method

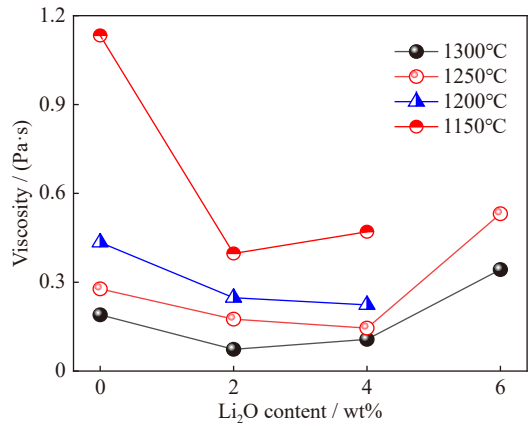


**Fig. 3. Effect of $Li_2O$ substituting for $B_2O_3$ on the mold flux viscosity.**

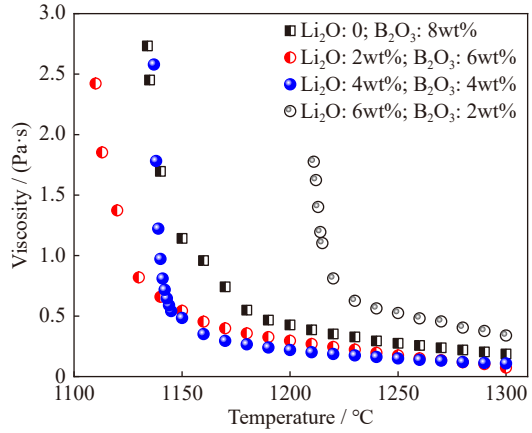


**Fig. 4. Viscosity–temperature curves of the mold flux with various $Li_2O$ and $B_2O_3$ contents.**

for estimating the break temperature of mold flux using the viscosity–temperature relationship. Eq. (1) is the Arrhenius equation, and Eq. (2) is obtained from Eq. (1) by taking the derivative of the reciprocal of the temperature. Eqs. (3) and (4) are derived from the first and second partial derivatives of the activation energy with respect to the temperature, respectively. When the second partial derivative equals 0, the temperature is defined as the break temperature [32].

$$\ln\eta = \ln A + \frac{E_a}{RT} \tag{1}$$

$$\frac{E_a}{R} = \frac{\partial \ln\eta}{\partial(1/T)} \tag{2}$$

$$\frac{1}{R}\frac{\partial E_a}{\partial T} = \frac{\partial\left(\frac{\partial \ln\eta}{\partial(1/T)}\right)}{\partial T} \tag{3}$$

$$\frac{1}{R}\frac{\partial^2 E_a}{\partial T^2} = \frac{\partial^2\left(\frac{\partial \ln\eta}{\partial(1/T)}\right)}{\partial T^2} \tag{4}$$

where $T$ is the temperature, °C; $\eta$ is the viscosity of the mold flux at $T$, Pa·s; $E_a$ is the activation energy of viscous flow, kJ/mol; $A$ is the apparent exponential prefactor; $R$ is the universal gas constant.

The break temperature calculation process is shown in Fig. 5. The melting point was measured using the hemispheric point method. Fig. 6 shows the variation in the melting point and break temperature of the mold flux. With increasing $Li_2O$ content in the mold flux, the melting point and break temperature first decreased and then increased, consistent with the evolution tendency of the viscosity. The combined addition of $B_2O_3$ and $Li_2O$ to the mold flux reduced the viscosity, melting point, and break temperature of the mold flux.

### 3.2. Effect of substituting $Li_2O$ for $B_2O_3$ on the structure of the mold flux

Aluminate and silicate network structures exist in the low-reactivity mold flux. The theory of silicate network structure is relatively mature [33–39]. The aluminate network structure is more complex than the silicate network structure. Aluminum has three coordination numbers of 4, 5, and 6, which form the network former ($[AlO_4]$ structural unit) and network modifier ($[AlO_5]$ and $[AlO_6]$ structural units), respectively. Scholars [40–42] used high-resolution solid-state NMR spectroscopy ($^{27}Al$ NMR) and molecular dynamics simulations to study the structural unit of the $CaO–Al_2O_3$ binary system and obtained consistent results. With the $CaO/Al_2O_3$ molar ratio greater than 1, the possibility of $[AlO_4]$ structural units being present in the highly peralkaline composition is higher. Two coordination environments enable the boron atom to form $[BO_4]$ and $[BO_3]$ structural units. The major structure in the borate structure is the two-dimensional boroxol ring, which is linked by the $[BO_3]$ triangular structure [24,43–44]. The three-dimensional borate structure is formed by the interconnection of the triangular $[BO_3]$ and tetrahedral $[BO_4]$ structural units [9,24,43–45]. With the addition of the above 30mol% network modifiers (including alkali metals and alkaline earth metals) to the mold flux, the $[BO_3]$ structural unit is dominant [46]. Because the content of network modifiers in the low-reactivity mold flux in the current study is higher than 60mol% [46], the borate network structure is mainly composed of $[BO_3]$ structural units.

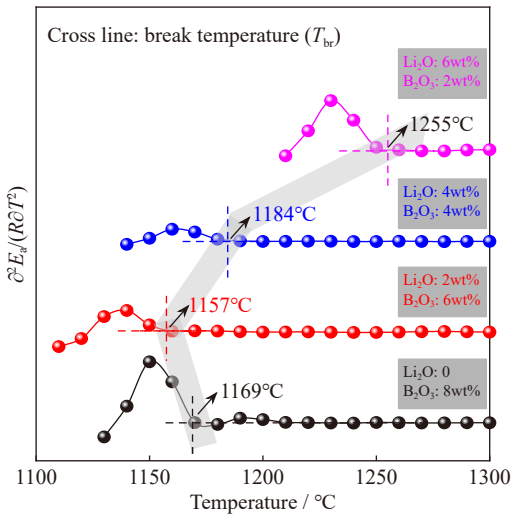


**Fig. 5. Calculation process of the break temperature.**

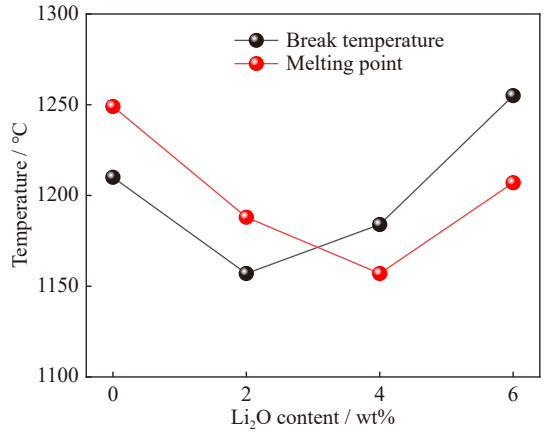


**Fig. 6. Melting point and break temperature of the mold flux with various $Li_2O$ and $B_2O_3$ contents.**

Assignments of the deconvoluted Raman bands are summarized in Table 3 [9,46–65]. The original and deconvoluted Raman spectra of mold fluxes with various $Li_2O$ and $B_2O_3$ contents are shown in Figs. 7 and 8. The related fractions of structural units are shown in Figs. 9 and 10. As $Li_2O$ replaced $B_2O_3$ in the mold flux, the fraction of $Al_{IV}–O–B_{III}$ structural units composed of $[BO_3]$ gradually decreased, and the total fraction of the borate structure decreased from approximately 18wt% to 10wt%. The borate structure decreased because of a reduction in $B_2O_3$ content in the mold flux. The fraction of the Al–F linkage decreased slightly with the substitution of $Li_2O$ for $B_2O_3$ in the mold flux. With the $Li_2O$ content of the mold flux increasing from 0 to 6wt%, the fraction of the Al–O–Al linkage increased from 6wt% to 12wt%, and the fraction of $Al–O^-$ decreased, indicating that the fraction of the bridging oxygen in the aluminate structure increased. The higher content of free oxygen ions ($O^{2-}$) generated by $Li_2O$ led to the breakage of the Si–O–Si linkage to

**Table 3. Assignments of deconvoluted Raman bands [9,46–65]**

| Raman shift / $cm^{-1}$ | Assignment | References |
|---|---|---|
| ~530 | Al–F stretching vibration ([$AlF_6$] octahedral structure) | [47–49] |
| 540–560 | Al–O–Al bending vibrations | [47,49–55] |
| 630–650 | $Al_{IV}$–O–$B_{III}$ bending vibration | [56–57] |
| 750–780 | Al–$O^-$ stretching vibration in $AlO_4$ units with 1 or 2 non-bridge oxygens | [47,50–51] |
| 830–850 | Al–O–Si linkage | [49] |
| 850–880 | $Q^0_{Si}$ | [58–61] |
| 900–920 | $Q^1_{Si}$ | [58–61] |
| 950–1000 | $Q^2_{Si}$ | [58–61] |
| 1200–1300 | B–$O^-$ linkage in pyroborate units ($[B_2O_5]^4$) | [62–64] |
| 1320–1340 | B–$O^-$ linkage in chain and ring metaborate units | [9,46,64–65] |

form the Si–$O^-$ linkage, reducing the degree of polymerization (DOP) of the silicate network structure in the CaO–$SiO_2$-based mold flux [66–67]. However, for the CaO–$Al_2O_3$–10wt%$SiO_2$-based low-reactivity mold flux, $Li_2O$ played a more important role as a charge compensator. With the $Li_2O$ in the mold flux increased, the Al–$O^-$ linkage-transformed Al–O–Al linkage was promoted. Meanwhile, the charge compensation of $Li^+$ between $Al^{3+}$ and $Si^{4+}$ could link the Al–$O^-$ and silicate structural units to form the Al–O–Si linkage with a higher DOP of the melt structure [18–19,21]. Correspondingly, the fraction of Al–O–Si increased, and the structural units of stretching vibrations of Si–O in $SiO_4^{4-}$ ($Q^2_{Si}$), $Si_2O_7^{6-}$($Q^1_{Si}$), and $SiO_3^{2-}$ ($Q^0_{Si}$) decreased.

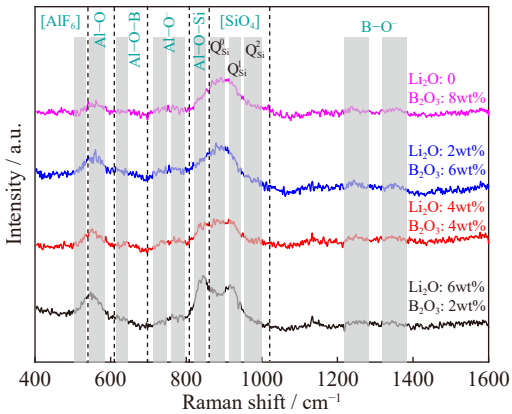


**Fig. 7. Original Raman spectra of mold fluxes with different $Li_2O$ and $B_2O_3$ contents.**

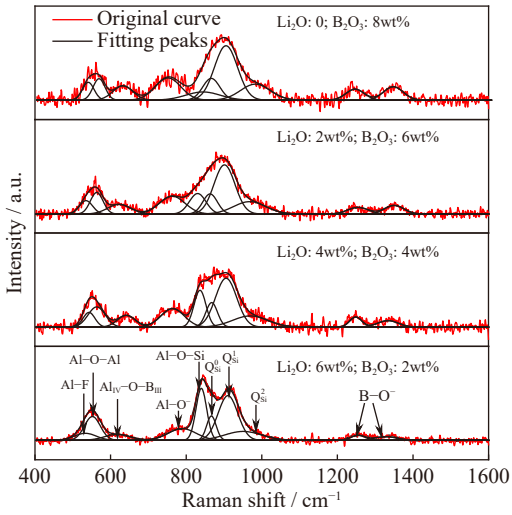


**Fig. 8. Deconvoluted Raman spectra of mold fluxes with various $Li_2O$ and $B_2O_3$ contents.**

### 3.3. Effect of substituting $Li_2O$ for $B_2O_3$ on the crystalline phase of the mold flux

Figs. 11 and 12 show the precipitation of crystalline

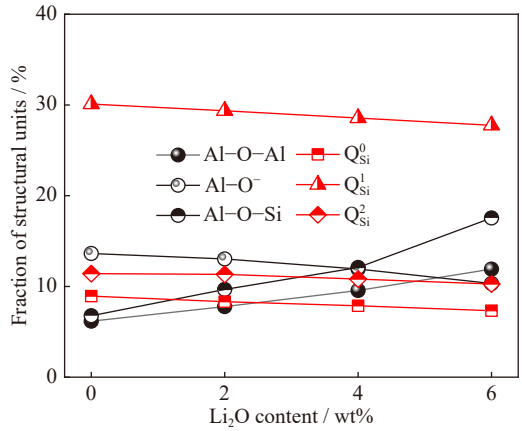


**Fig. 9. Fraction of aluminate and silicate structural units of mold fluxes with various $Li_2O$ and $B_2O_3$ contents.**

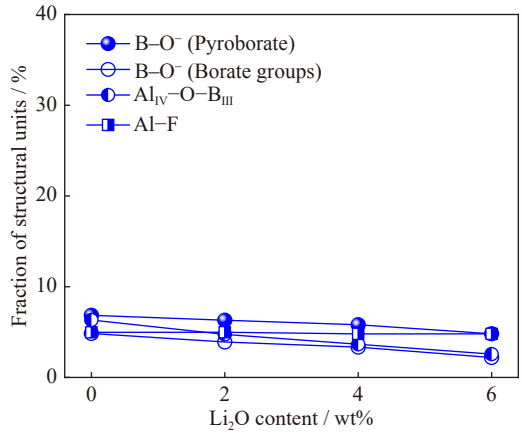


**Fig. 10. Fraction of other structural units of mold fluxes with various $Li_2O$ and $B_2O_3$ contents.**

phases in mold fluxes with different $Li_2O$ and $B_2O_3$ contents at 1150 and 950°C. Crystalline phases in the mold flux substantially increased as the temperature decreased from 1150 and 950°C. The replacement of $B_2O_3$ by $Li_2O$ in the mold flux promoted the precipitation of $CaF_2$, $LiAlO_2$, and $11CaO{\cdot}7Al_2O_3{\cdot}CaF_2$ crystals and inhibited the precipitation of $2CaO{\cdot}Al_2O_3{\cdot}SiO_2$ crystals. A higher $B_2O_3$ content in the mold flux retarded $CaF_2$ phase precipitation, consistent with previous studies by Yang *et al.* [31] and Xiao *et al.* [68]. With the content of $Li_2O$ more than 2wt%, the high melting point

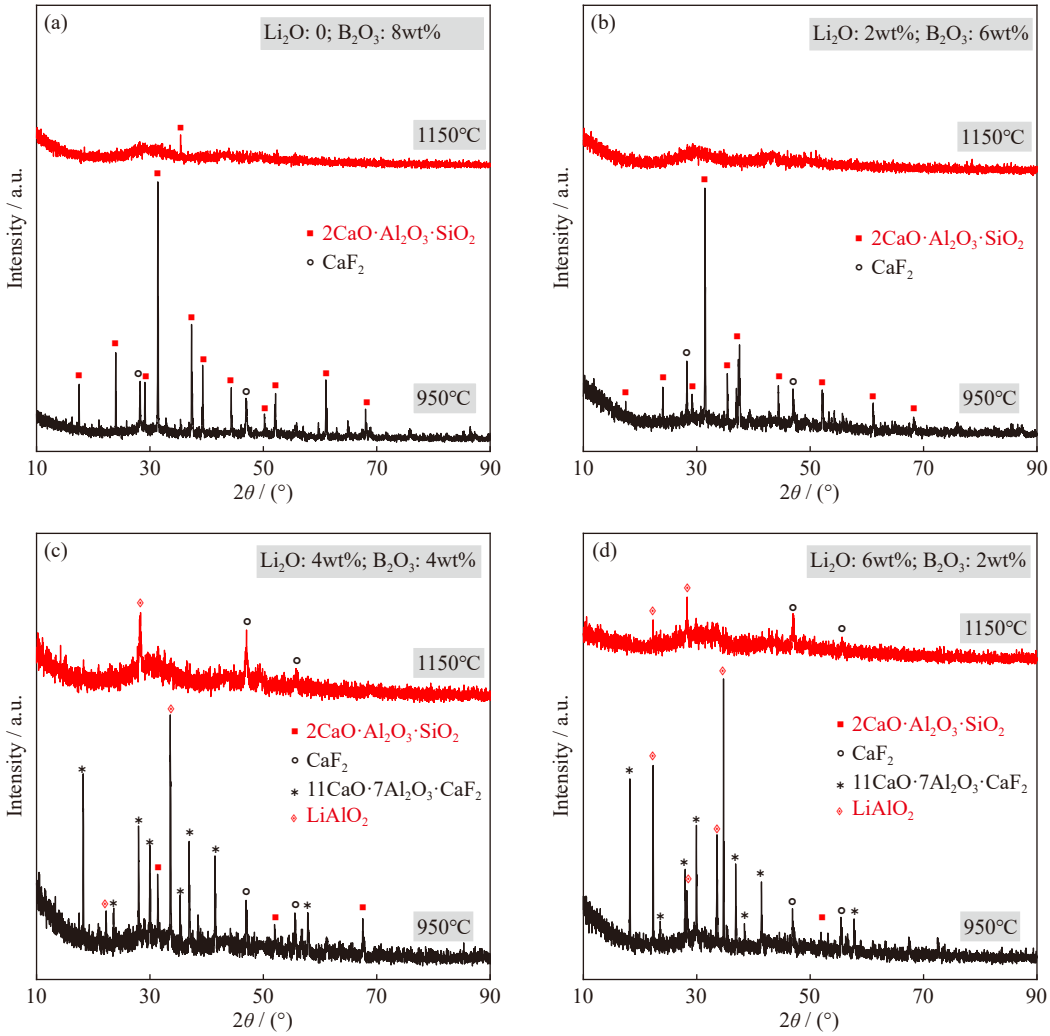


**Fig. 11. Effect of various $Li_2O$ and $B_2O_3$ contents on the crystalline phase of the mold flux. (a) $Li_2O$: 0, $B_2O_3$: 8wt%; (b) $Li_2O$: 2wt%, $B_2O_3$: 6wt%;(c) $Li_2O$: 4wt%, $B_2O_3$: 4wt%; (d) $Li_2O$: 6wt%, $B_2O_3$: 2wt%.**

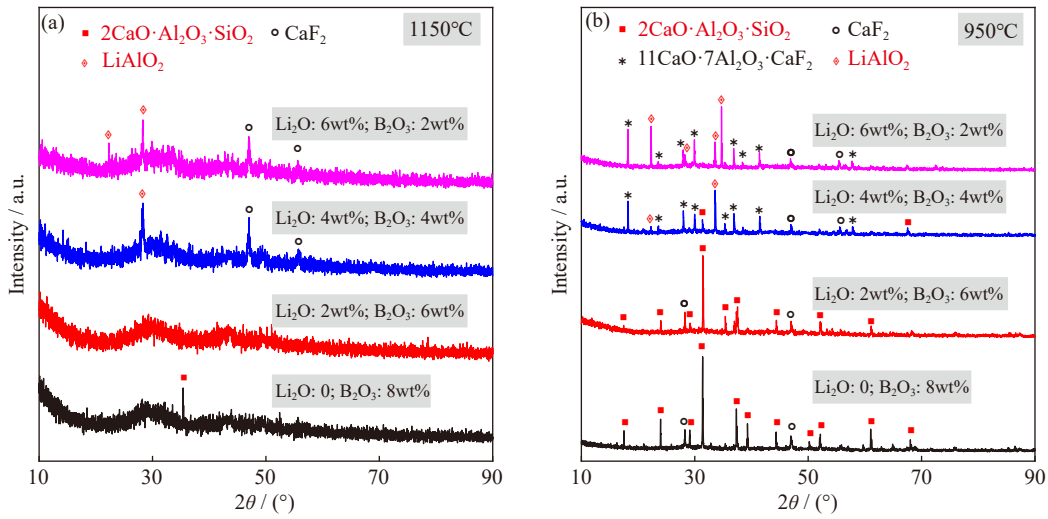


**Fig. 12. Effect of $Li_2O$ replacing $B_2O_3$ on the crystalline phase of the mold flux at different temperatures (a) 1150°C; (b) 950°C.**

crystalline phase of $LiAlO_2$ (1700°C) gradually precipitated. The $LiAlO_2$ phase easily precipitated in the $CaO–Al_2O_3$ slag system because of its structural characteristics [45,69–70]. The precipitated $LiAlO_2$ increased the viscosity and worsened the crystallization tendency of the mold flux [19–20]. As the $Li_2O$ content in the mold flux increased from 0 to 6wt%, the crystallization tendency of the mold flux first decreased and then increased at 1150°C. Notably, the mold flux with 2wt% $Li_2O$ and 6wt% $B_2O_3$ was the pure liquid phase at 1150°C.

$LiAlO_2$ crystal formation required the charge compensation effect of $Li^+$ on the aluminate structure; thus, with increasing $Li_2O$ content in the mold flux, $Li^+$ replaced metal cations such as $Ca^{2+}$ in the $[AlO_4]$ structural unit [21]. As the $Li_2O$ content of the mold flux increased from 0 to 6wt%, $Li_2O$ strengthened the aluminate network structure through $Li^+$, while $LiAlO_2$ crystals gradually precipitated in the mold flux. This result was consistent with the Raman spectroscopy results. In summary, mold flux viscosity first decreased and then increased with the substitution of $Li_2O$ for $B_2O_3$ in the mold flux. The melt structure and precipitated crystalline phase caused the evolution of viscosity. The precipitation of crystalline phases and the higher DOP increased the viscosity of the mold flux. The addition of 2wt% $Li_2O$ and 6wt% $B_2O_3$ to the mold flux reduced the reactivity, viscosity, and melting point of the mold flux and lowered the crystallization tendency of the mold flux in the high-temperature zone. The combined addition of $Li_2O$ and $B_2O_3$ to the mold flux improved the properties of the mold flux of high-aluminum steels.

## 4. Conclusions

In this study, the evolution of viscosity, melt structure, and crystalline phase of the mold flux with the replacement of $B_2O_3$ by $Li_2O$ from 0 to 6wt% was investigated. The main results are summarized as follows.

(1) The combined addition of $Li_2O$ and $B_2O_3$ with appropriate proportion was beneficial to reduced the viscosity, melting point, and break temperature of the low-reactivity mold flux. The viscosity reached a minimum of 0.07 Pa·s with 2wt% $Li_2O$ and 6wt% $B_2O_3$ in the mold flux.

(2) An increase in $Li_2O$ content in the mold flux from 0 to 6wt% strengthened aluminate and aluminosilicate structures by increasing $Li^+$ released from $Li_2O$. Meanwhile, the proportion of silicate structural units decreased.

(3) The replacement of $B_2O_3$ by $Li_2O$ in the mold flux promoted $LiAlO_2$ precipitation, and a $Li_2O$ content of no more than 2wt% is suggested to avoid $LiAlO_2$ phase precipitation.

## Acknowledgements

This work was financially supported by the National Science Foundation China (No. U22A20171) and the Scinence and Technology Program of Hebei, China (No. 20311004D). We also appreciate the other support from High Steel Center (HSC) at North China University of Technology, Yanshan University, University of Science and Technology Beijing, Hebei Innovation Center of the Development and Application of High Quality Steel Materials, China, and Hebei International Research Center of Advanced and Intelligent Manufacturing of High Quality Steel Materials, China.

## Conflict of Interest

The authors declare no conflict of interest.

## References

[1] X.J. Fu, G.H. Wen, P. Tang, Q. Liu, and Z.Y. Zhou, Effects of $CaO/Al_2O_3$ ratio on crystallisation behaviour of $CaO–Al_2O_3$ based mould fluxes for high aluminium TRIP steel, *Ironmaking Steelmaking*, 41(2014), No. 5, p. 342.

[2] H.X. Yu, D.X. Yang, J.M. Zhang, G.Y. Qiu, and N. Zhang, Effect of Al content on the reaction between Fe–10Mn–*x*Al (*x* = 0.035wt%, 0.5wt%, 1wt%, and 2wt%) steel and $CaO–SiO_2–Al_2O_3–MgO$ slag, *Int. J. Miner. Metall. Mater.*, 29(2022), No. 2, p. 256.

[3] Y. Chen, S.P. He, Z.R. Li, X.B. Zhang, Q.Q. Wang, and Q. Wang, Properties and structure of a new non-reactive mold flux for high-Al steel, *J. Iron Steel Res. Int.*, 29(2022), No. 1, p. 61.

[4] M.S. Kim and Y.B. Kang, A reaction model to simulate composition change of mold flux during continuous casting of high Al steel, [in] R.G. Reddy, P. Chaubal, P.C. Pistorius, U. Pal, eds, *Advances in Molten Slags, Fluxes, and Salts: Proceedings of the 10th International Conference on Molten Slags, Fluxes and Salts 2016*, Springer, Cham, 2016, p. 271.

[5] M.S. Kim, M.S. Park, and Y.B. Kang, A reaction between high Mn-high Al steel and $CaO–SiO_2$-type molten mold flux: Reduction of additive oxide components in mold flux by Al in steel, *Metall. Mater. Trans. B*, 50(2019), No. 5, p. 2077.

[6] M.S. Kim, M.S. Park, S.E. Kang, J.K. Park, and Y.B. Kang, A reaction between high Mn–high Al steel and $CaO–SiO_2$-type molten mold flux: Reaction mechanism change by high Al content ($[pct\ Al]_0 = 5.2$) in the steel and accumulation of reaction product at the reaction interface, *ISIJ Int.*, 58(2018), No. 4, p. 686.

[7] M.S. Kim, S.W. Lee, J.W. Cho, M.S. Park, H.G. Lee, and Y.B. Kang, A reaction between high Mn-high Al steel and $CaO–SiO_2$-type molten mold flux: Part I. composition evolution in molten mold flux, *Metall. Mater. Trans. B*, 44(2013), No. 2, p. 299.

[8] Y.M. Gao, S.B. Wang, C. Hong, X.J. Ma, and F. Yang, Effects of basicity and MgO content on the viscosity of the $SiO_2–CaO–MgO–9wt\%Al_2O_3$ slag system, *Int. J. Miner. Metall. Mater.*, 21(2014), No. 4, p. 353.

[9] G.H. Kim and I. Sohn, Role of $B_2O_3$ on the viscosity and structure in the $CaO–Al_2O_3–Na_2O$-based system, *Metall. Mater. Trans. B*, 45(2014), No. 1, p. 86.

[10] S.P. He, Z.R. Li, Z. Chen, T. Wu, and Q. Wang, Review of mold fluxes for continuous casting of high-alloy (Al, Mn, Ti) steels, *Steel Res. Int.*, 90(2019), No. 1, art. No. 1800424.

[11] S. Street, K. James, N. Minor, A. Roelant, and J. Tremp, Production of high-aluminum steel slabs, *Iron Steel Technol.*, 5(2008), No. 7, p. 38.

[12] C.X. Ji, Y. Cui, Z. Zeng, Z.H. Tian, C.L. Zhao, and G.S. Zhu, Continuous casting of high-Al steel in Shougang Jingtang steel works, *J. Iron Steel Res. Int.*, 22(2015), No. 1, p. 53.

[13] H. Wang, *Study on Crystallization Behaviors and Heat Transfer of High Al Steel Mould Fluxes* [Dissertation], Chongqing

university, Chongqing, 2010.
[14] H. Wang, P. Tang, G.H. Wen, and X. Yu, Effect of $Na_2O$ on crystallisation behaviour and heat transfer of high Al steel mould fluxes, *Ironmaking Steelmaking*, 38(2011), No. 5, p. 369.
[15] T. Wu, S.P. He, L.L. Zhu, and Q. Wang, Study on reaction performances and applications of mold flux for high-aluminum steel, *Mater. Trans.*, 57(2016), No. 1, p. 58.
[16] K. Blazek, H.B. Yin, G. Skoczylas, M. McClymonds, and M. Frazee, Development and evaluation of lime alumina-based mold powders for casting high-aluminum TRIP steel grades, [in] *AISTech, Iron and Steel Technology Conference and Exhibition*, 2011, p. 1577.
[17] J.M. Li, M.F. Jiang, and L.F. Sun, Development of low responsiveness mold fluxes for 20$Mn_{23}$AlV, *China Metall.*, 27(2017), No. 12, p. 28.
[18] H.M. Wang, T.W. Zhang, H. Zhu, G.R. Li, Y.Q. Yan, and J.H. Wang, Effect of $B_2O_3$ on melting temperature, viscosity and desulfurization capacity of CaO-based refining flux, *ISIJ Int.*, 51(2011), No. 5, p. 702.
[19] J.L. Li, B.W. Kong, B. Galdino, *et al.*, Investigation on properties of fluorine-free mold fluxes based on CaO–$Al_2O_3$–$B_2O_3$ system, *Steel Res. Int.*, 88(2017), No. 9, art. No. 1600485.
[20] W. Yan, W.Q. Chen, Y.D. Yang, and A. McLean, Viscous characteristics and modelling of CaO–$Al_2O_3$–based mould flux with $B_2O_3$ as a substitute for $CaF_2$, *Ironmaking Steelmaking*, 46(2019), No. 4, p. 347.
[21] W. Yan, W. Chen, Y. Yang, C. Lippold, and A. McLean, Evaluation of $B_2O_3$ as replacement for $CaF_2$ in CaO–$Al_2O_3$ based mould flux, *Ironmaking Steelmaking*, 43(2016), No. 4, p. 316.
[22] X. Yu, G.H. Wen, P. Tang, and H. Wang, Effect of $B_2O_3$ on the physico-chemical properties of mold slag used for high-Al steel, *J. Chongqing Univ.*, 34(2011), No. 1, p. 66.
[23] X.H. Huang, J.L. Liao, K. Zheng, H.H. Hu, F.M. Wang, and Z.T. Zhang, Effect of $B_2O_3$ addition on viscosity of mould slag containing low silica content, *Ironmaking Steelmaking*, 41(2014), No. 1, p. 67.
[24] G.H. Kim and I. Sohn, Influence of $Li_2O$ on the viscous behavior of CaO–$Al_2O_3$–12 mass% $Na_2O$–12 mass% $CaF_2$ based slags, *ISIJ Int.*, 52(2012), No. 1, p. 68.
[25] T. Wu, Q. Wang, S.P. He, J.F. Xu, X. Long, and Y.J. Lu, Study on properties of alumina-based mould fluxes for high-Al steel slab casting, *Steel Res. Int.*, 83(2012), No. 12, p. 1194.
[26] J.L. Li, B.W. Kong, X.Y. Gao, Q.C. Liu, Q.F. Shu, and K. Chou, Investigation the influences of $B_2O_3$ and $R_2O$ on the structure and crystallization behaviors of CaO–$Al_2O_3$ based F-free mold flux, *Metall. Res. Technol.*, 115(2018), No. 3, art. No. 304.
[27] J. Qi, C. Liu, and M. Jiang, Role of $Li_2O$ on the structure and viscosity in CaO–$Al_2O_3$–$Li_2O$–$Ce_2O_3$ melts, *J. Non Cryst. Solids*, 475(2017), p. 101.
[28] L.J. Zhou, H. Li, W.L. Wang, D. Xiao, L. Zhang, and J. Yu, Effect of $Li_2O$ on the behavior of melting, crystallization, and structure for CaO–$Al_2O_3$-based mold fluxes, *Metall. Mater. Trans. B*, 49(2018), No. 5, p. 2232.
[29] B.X. Lu, K. Chen, W.L. Wang, and B.B. Jiang, Effects of $Li_2O$ and $Na_2O$ on the crystallization behavior of lime–alumina-based mold flux for casting high-Al steels, *Metall. Mater. Trans. B*, 45(2014), No. 4, p. 1496.
[30] J. Qi, C.J. Liu, C.L. Li, and M.F. Jiang, Viscous properties of new mould flux based on aluminate system with $CeO_2$ for continuous casting of RE alloyed heat resistant steel, *J. Rare Earths*, 34(2016), No. 3, p. 328.
[31] J. Yang, H. Cui, J. Zhang, O. Ostrovski, C. Zhang, and D. Cai, Effect of $Na_2O$ on the interfacial reaction between CaO–$Al_2O_3$ based mold fluxes and high-Al steel at 1500°C, *ISIJ Int.*, 59(2019), No. 12, p. 2247.
[32] S. Seftharaman, S.C. Du, S. Sridhar, and K.C. Mills, Estimation of liquidus temperatures for multicomponent silicates from activation energies for viscous flow, *Metall. Mater. Trans. B*, 31(2000), No. 1, p. 111.
[33] J.Y. Chen, W.L. Wang, L.J. Zhou, and Z.H. Pan, Effect of $Al_2O_3$ and MgO on crystallization and structure of CaO–$SiO_2$–$B_2O_3$-based fluorine-free mold flux, *J. Iron Steel Res. Int.*, 28(2021), No. 5, p. 552.
[34] J.T. Ju, K.S. Yang, Z.H. Zhu, Y. Gu, and L.Z. Chang, Effect of $CaF_2$ and CaO/$Al_2O_3$ on viscosity and structure of $TiO_2$-bearing slag for electroslag remelting, *J. Iron Steel Res. Int.*, 28(2021), No. 12, p. 1541.
[35] F. Yuan, Z. Zhao, Y.L. Zhang, and T. Wu, Influence of $Cr_2O_3$ content on viscosity and rheological behavior of $Cr_2O_3$-containing slags, *J. Iron Steel Res. Int.*, 29(2022), No. 4, p. 601.
[36] D.L. Zheng, G.J. Ma, X. Zhang, M.K. Liu, and J. Xu, Effect of CaO/$Al_2O_3$ on structure, viscosity, and surface tension of electroslag remelting-type $CeO_2$-bearing slag, *J. Iron Steel Res. Int.*, (2022), p. 1.
[37] L.J. Zhou, H. Luo, W.L. Wang, X. Yan, and H.F. Wu, Effect of $Al_2O_3$/$Na_2O$ ratio and MnO on high-temperature properties of mold flux for casting peritectic steel, *J. Iron Steel Res. Int.*, 29(2022), No. 1, p. 53.
[38] F. Yuan, Z. Zhao, Y.L. Zhang, and T. Wu, Effect of $Al_2O_3$ content on the viscosity and structure of CaO–$SiO_2$–$Cr_2O_3$–$Al_2O_3$ slags, *Int. J. Miner. Metall. Mater.*, 29(2022), No. 8, p. 1522.
[39] C.Y. Xu, C. Wang, R.Z. Xu, J.L. Zhang, and K.X. Jiao, Effect of $Al_2O_3$ on the viscosity of CaO–$SiO_2$–$Al_2O_3$–MgO–$Cr_2O_3$ slags, *Int. J. Miner. Metall. Mater.*, 28(2021), No. 5, p. 797.
[40] B.T. Poe, P.F. McMillan, B. Coté, D. Massiot, and J.P. Coutures, Structure and dynamics in calcium aluminate liquids: High-temperature 27Al NMR and Raman spectroscopy, *J. Am. Ceram. Soc.*, 77(1994), No. 7, p. 1832.
[41] P.F. McMillan, W.T. Petuskey, B. Coté, D. Massiot, C. Landron, and J.P. Coutures, A structural investigation of CaO–$Al_2O_3$ glasses via 27Al MAS-NMR, *J. Non Cryst. Solids*, 195(1996), No. 3, p. 261.
[42] D.R. Neuville, L. Cormier, and D. Massiot, Al coordination and speciation in calcium aluminosilicate glasses: Effects of composition determined by $^{27}$Al MQ-MAS NMR and Raman spectroscopy, *Chem. Geol.*, 229(2006), No. 1-3, p. 173.
[43] V.P. Klyuev and B.Z. Pevzner, The influence of aluminum oxide on the thermal expansion, glass transition temperature, and viscosity of lithium and sodium aluminoborate glasses, *Glass Phys. Chem.*, 28(2002), No. 4, p. 207.
[44] V.P. Klyuev and B. Pevzner, Structural interpretation of the glass transition temperature and thermal expansion of glasses in the system BaO–$Al_2O_3$–$B_2O_3$, *Phys. Chem. Glasses*, 41(2000), p. 380.
[45] J. Qi, C.J. Liu, and M.F. Jiang, Viscosity–structure–crystallization of the $Ce_2O_3$-bearing calcium-aluminate-based melts with different contents of $B_2O_3$, *ISIJ Int.*, 58(2018), No. 1, p. 186.
[46] G. Padmaja and P. Kistaiah, Infrared and Raman spectroscopic studies on alkali borate glasses: Evidence of mixed alkali effect, *J. Phys. Chem. A*, 113(2009), No. 11, p. 2397.
[47] J.H. Park, D.J. Min, and H.S. Song, Structural investigation of CaO–$Al_2O_3$ and CaO–$Al_2O_3$–$CaF_2$ slags via Fourier transform infrared spectra, *ISIJ Int.*, 42(2002), No. 1, p. 38.
[48] N. Ma, J.L. You, L.M. Lu, J. Wang, M. Wang, and S.M. Wan, Micro-structure studies of the molten binary $K_3AlF_6$–$Al_2O_3$ system by *in situ* high temperature Raman spectroscopy and theoretical simulation, *Inorg. Chem. Front.*, 5(2018), No. 8, p. 1861.
[49] J. Yang, J.Q. Zhang, O. Ostrovski, C. Zhang, and D.X. Cai, Effects of fluorine on solidification, viscosity, structure, and heat transfer of CaO–$Al_2O_3$-based mold fluxes, *Metall. Mater. Trans. B*, 50(2019), No. 4, p. 1766.
[50] P. McMillan and B. Piriou, Raman spectroscopy of calcium aluminate glasses and crystals, *J. Non Cryst. Solids*, 55(1983), No.

2, p. 221.
[51] T.S. Kim and J.H. Park, Structure–viscosity relationship of low-silica calcium aluminosilicate melts, *ISIJ Int.*, 54(2014), No. 9, p. 2031.
[52] H. Li, P. Hrma, J.D. Vienna, M.X. Qian, Y.L. Su, and D.E. Smith, Effects of $Al_2O_3$, $B_2O_3$, $Na_2O$, and $SiO_2$ on nepheline formation in borosilicate glasses: Chemical and physical correlations, *J. Non Cryst. Solids*, 331(2003), No. 1-3, p. 202.
[53] E.Z. Gao, W.L. Wang , and L. Zhang, Effect of alkaline earth metal oxides on the viscosity and structure of the CaO–$Al_2O_3$ based mold flux for casting high-al steels, *J. Non Cryst. Solids*, 473(2017), p. 79.
[54] J.X. Gao, G.H. Wen, T. Huang, B.W. Bai, P. Tang, and Q. Liu, Effect of Al speciation on the structure of high-Al steels mold fluxes containing fluoride, *J. Am. Ceram. Soc.*, 99(2016), No. 12, p. 3941.
[55] G.H. Kim and I. Sohn, Effect of $Al_2O_3$ on the viscosity and structure of calcium silicate-based melts containing $Na_2O$ and $CaF_2$, *J. Non Cryst. Solids*, 358(2012), No. 12-13, p. 1530.
[56] R. El Hayek, F. Ferey, P. Florian, A. Pisch, and D.R. Neuville, Structure and properties of lime alumino-borate glasses, *Chem. Geol.*, 461(2017), p. 75.
[57] L.S. Du and J.F. Stebbins, Site connectivities in sodium aluminoborate glasses: Multinuclear and multiple quantum NMR results, *Solid State Nucl. Magn. Reson.*, 27(2005), No. 1-2, p. 37.
[58] D.R. Neuville, G.S. Henderson, L. Cormier, and D. Massiot, The structure of crystals, glasses, and melts along the CaO–$Al_2O_3$ join: Results from Raman, Al *L*- and *K*-edge X-ray absorption, and $^{27}$Al NMR spectroscopy, *Am. Mineral.*, 95(2010), No. 10, p. 1580.
[59] P. McMillan, Structural studies of silicate glasses and melts—Applications and limitations of Raman spectroscopy, *Am. Mineral.*, 69(1984), No. 7-8, p. 622.
[60] B.O. Mysen and D. Virgo, Structure and properties of fluorine-bearing aluminosilicate melts: The system $Na_2O$–$Al_2O_3$–$SiO_2$–F at 1 atm, *Contr. Mineral. Petrol.*, 91(1985), No. 3, p. 205.
[61] J.Y. Park, G.H. Kim, J.B. Kim, S. Park, and I. Sohn, Thermophysical properties of $B_2O_3$-containing mold flux for high carbon steels in thin slab continuous casters: Structure, viscosity, crystallization, and wettability, *Metall. Mater. Trans. B*, 47(2016), No. 4, p. 2582.
[62] B.P. Dwivedi and B.N. Khanna, Cation dependence of Raman scattering in alkali borate glasses, *J. Phys. Chem. Solids*, 56(1995), No. 1, p. 39.
[63] H. Li, Y.L. Su, L.Y. Li, and D.M. Strachan, Raman spectroscopic study of gadolinium(III) in sodium-aluminoborosilicate glasses, *J. Non Cryst. Solids*, 292(2001), No. 1-3, p. 167.
[64] E.I. Kamitsos, M.A. Karakassides, and G.D. Chryssikos, Vibrational spectra of magnesium–sodium–borate glasses. 2. Raman and mid-infrared investigation of the network structure, *J. Phys. Chem.*, 91(1987), No. 5, p. 1073.
[65] Y. Kim and K. Morita, Relationship between molten oxide structure and thermal conductivity in the CaO–$SiO_2$–$B_2O_3$ system, *ISIJ Int.*, 54(2014), No. 9, p. 2077.
[66] X.D. Xing, Z.G. Pang, C. Mo, S. Wang, and J.T. Ju, Effect of MgO and BaO on viscosity and structure of blast furnace slag, *J. Non Cryst. Solids*, 530(2020), art. No. 119801.
[67] L. Zhang, W.L. Wang, S.L. Xie, K.X. Zhang, and I. Sohn, Effect of basicity and $B_2O_3$ on the viscosity and structure of fluorine-free mold flux, *J. Non Cryst. Solids*, 460(2017), p. 113.
[68] D. Xiao, W.L. Wang, and B.X. Lu, Effects of $B_2O_3$ and BaO on the crystallization behavior of CaO–$Al_2O_3$-based mold flux for casting high-Al steels, *Metall. Mater. Trans. B*, 46(2015), No. 2, p. 873.
[69] W. Yan, W. Chen, Y. Yang, C. Lippold, and A. McLean, Effect of CaO/$Al_2O_3$ ratio on viscosity and crystallisation behaviour of mould flux for high Al non-magnetic steel, *Ironmaking Steelmaking*, 42(2015), No. 9, p. 698.
[70] Q. Wang, J. Yang, C. Zhang, D.X. Cai, J.Q. Zhang, and O. Ostrovski, Effect of CaO/$Al_2O_3$ ratio on viscosity and structure of CaO–$Al_2O_3$-based fluoride-free mould fluxes, *J. Iron Steel Res. Int.*, 26(2019), No. 4, p. 374.